

Modeling Mixing near HE-Air Interfaces in Explosions

Allen L. Kuhl and David Grote
Lawrence Livermore National Laboratory
Livermore, California USA

John B. Bell and Vincent E. Beckner
Lawrence Berkeley National Laboratory
Berkeley, California USA

1 Introduction

We consider the problem of mixing near HE-air interfaces in explosions, where the Detonation Products (DP) are rich in carbon particles (Fig. 1). The model consists of gas phase conservation laws (i.e., the compressible Navier-Stokes equations), coupled with a heterogeneous continuum model for the carbon particle phase. The problem is assumed to be point symmetric, so the 1D spherical coordinates are used. The hyperbolic terms are integrated with a 2nd-order Godunov scheme (PPM), while the viscous terms are advanced by a 2nd-order Runge-Kutta method. The particle phase conservation laws are also integrated with a 2nd-order Godunov scheme for dilute particle systems (Collins, 1994). Adaptive Mesh Refinement is used to resolve steep gradients in the flow. A tabular EOS is used (Fig. 2), based on equilibrium thermodynamics (Cheetah code). Three converged solutions were found: (i) inviscid, (ii) viscous and (iii) two-phase. The blast wave solution (p, ρ, T, u_r) scaled gasdynamically (i.e., r & $t \sim cm/g^{1/3}$), however, the DP-Air interface and peak temperature were smeared by molecular diffusion effects. Similarity solutions for the latter show that diffusion effects scale with the appropriately-defined Peclet and Reynolds numbers.

2 Model

2.1 Gas Phase Conservation Laws: compressible Navier-Stokes equations for 1D point-symmetric flow

$$\text{Mass} \quad \partial_t \rho + \nabla_r \cdot (\rho u_r) = 0 \quad (1)$$

$$\text{Momentum:} \quad \partial_t \rho u_r + \nabla_r \cdot (\rho u_r u_r + p) = \nabla_r \cdot (2\mu + \lambda) \nabla_r u_r - D \quad (2)$$

$$\text{Energy:} \quad \partial_t \rho E + \nabla_r \cdot (\rho E u_r + p u_r) = \nabla_r \cdot u_r (2\mu + \lambda) \nabla_r u_r + \nabla_r \cdot \kappa \nabla_r T + \nabla \cdot h_D \rho D_m \nabla Y_D - Q - D \cdot u_r \quad (3)$$

$$\text{Products:} \quad \partial_t \rho Y_D + \nabla_r \cdot (\rho Y_D u_r) = \nabla_r \cdot (\rho D_m \nabla_r Y_D) \quad \text{with} \quad Y_D + Y_A = 1 \quad (4)$$

$$\text{Constitutive Law:} \quad \sigma_{ij} = (2\mu + \lambda) e_{ii} - \nabla p \delta_{ij} \quad (5)$$

$$\text{EOS:} \quad p, T, \Gamma = f_i(\rho, u, Y_D) \quad (\text{Cheetah code}) \quad (6)$$

Correspondence to: kuhl2@llnl.gov

$$\text{Transport: } \mu, \lambda, \kappa, D_m = g_i(\rho, u, Y_D) \text{ with } Le \equiv \lambda / \rho c_p D_m = 1 \quad (\text{Cheetah code}) \quad (7)$$

$$\text{Divergence: } \nabla_r \cdot (\cdot) \equiv \frac{3}{r^3} \frac{\partial}{\partial r} r^2 (\cdot) \quad \& \quad e_{ii} = \{\partial_r u_r, u_r / r, u_r / r\} \quad (1\text{-D spherical coordinates}) \quad (8)$$

2.2 Particle Phase Conservation Laws: Heterogeneous Continuum Model (Nigmatulin, 1991)

$$\text{Mass: } \partial_t \sigma + \nabla_r \cdot \sigma v_r = 0 \quad (9)$$

$$\text{Momentum: } \partial_t \sigma v_r + \nabla_r \cdot \sigma v_r v_r = D \quad (10)$$

$$\text{Energy: } \partial_t \sigma E_s + \nabla_r \cdot \sigma E_s v_r = Q + D \cdot u_r \quad \text{where } E_s = c_s T_s \quad \& \quad p_s = 0 \quad (11)$$

$$\text{Drag: } D = (1/8) \pi d^2 \rho (u_r - v_r) |u_r - v_r| C_D \quad \text{where } C_D = 0.48 + 28 Re^{-0.85} \quad (12)$$

$$\text{Heat Transfer: } Q_p = \pi d \mu C_p Pr^{-1} (T - T_s) Nu \quad \text{where } Nu = 2 + 0.6 Pr^{1/3} Re^{1/2} \quad (13)$$

2.3 Numerical Methods—The hyperbolic terms in the conservation laws, i.e. the left-hand side of eqs. (1-4), were integrated with a 2nd-order Godunov scheme (PPM); the Navier-Stokes terms, i.e., the right-hand side of eqs. (1-4) were integrated with a 2nd-order Runge-Kutta method. The particle-phase conservation laws, i.e., eqs. (9-11), were integrated with a 2nd-order Godunov scheme, developed for dilute particle systems (Collins et al., 1994). The source terms of drag and heat transfer were advanced with a stiff ODE solver. Adaptive Mesh Refinement (Bell et al., 1994) was used to capture steep gradients on the computational mesh.

2.4 Initial Conditions—We assumed center-detonated spherical charges of TNT. Two charge masses were studied: 1-g and 1-kg. We also assumed that the detonation wave propagated at a constant velocity, corresponding the Chapman-Jouguet (CJ) state. In this case the detonation wave structure is described by a similarity solution (Kuhl, 2015). The similarity solution curves were multiplied by the CJ state variables and mapped on to the 1-D AMR grid to initialize the problem.

3 Solution

3.1 Temperature Profiles—Predicted temperature profiles are presented in Fig. 3a at $t = 10 \mu s$. The inviscid solution (black circles) shows ~ 3 cells in shock (as is typical of our Godunov schemes). The contact surface at $r = 3.7 cm$ contains ~ 30 cells, and the temperature rises to a peak value of $\sim 9,000$ K. Molecular diffusion spreads the profile and reduces the peak to 4,200 K (the viscous solution is red curve). The gas temperature profile predicted by the 2-phase model (blue curve) closely follows the inviscid solution; its dust temperature (green dashed curve) lies around 1,000 K, being in approximate temperature equilibrium with the detonation products gases.

3.2 Density Profiles—Predicted density profiles are presented in Fig. 3b at $t = 10 \mu s$. The inviscid solution (black circles) again shows ~ 3 cells in shock. The two-phase gas solution (blue curve) lies on top of the inviscid solution. The contact surface at $r = 3.7 cm$ contains ~ 30 cells. Molecular diffusion has spread the DP-air contact surface (red curve), forming a trough between the DP gases and air. The density of the particle phase (green curve) is an order of magnitude smaller than the gas phase. Also shown is the density profile (red circles) from the viscous model at $t = 20 \mu s$. Molecular viscosity has broadened both shocks and the contact surface to more than 100 cells.

3.3 Pressure Profiles—Predicted pressure profiles are presented in Fig. 3c at $t = 10 \mu s$. The viscous and 2-phase solutions lie on top of the inviscid solution. Although viscosity broadens the shock width, the peak pressures seem un-effected. The viscous solution at $t = 20 \mu s$ allows one to visualize the number of mesh points in the various discontinuities.

3.4 Velocity Profiles—Predicted velocity profiles are presented in Fig. 3d at $t = 10 \mu s$. As in the pressure case, the viscous (red curve) and gas 2-phase (blue curve) solutions lie on top of the inviscid solution (black circles). The dust velocity profile (green dashed curve) lags the air shock, and is $\sim 6\%$ less than the gas velocity profiles. The viscous solution (red circles) at $t = 20 \mu s$ allows one to visualize the number of mesh points in the main shock at $r = 6 \text{ cm}$ and embedded shock at $r = 5 \text{ cm}$.

3.5 Contact Surface—Predicted contact-surface (CS) profiles are presented in Fig. 3e at $t = 10 \mu s$. There one can see that the inviscid (black curve) and 2-phase (blue curve) models predict a discontinuous jump at the CS. However, the viscous solution (red curve) shows that molecular diffusion spreads the contact surface in space. We define a mixing layer width by: $\delta \equiv r(Y_D = 10\%) - r(Y_D = 90\%)$. The growth of the mixing layer width with time is presented in Fig. 3f. The curve fit shows that the mixing layer grows as t^2 in time. The number of cells in the mixing layer seems to grow approximately linearly with time. At $t = 0.63 \mu s$, there are about 144 cells in the mixing layer for a 1-gram charge and 164 cells for a 1-kg charge.

3.6 Scaling Laws—To analyze the solution, we adopt a heuristic, “predictor-corrector” point of view. In the “predictor step”, we integrate the inviscid conservation equations: $\partial_t U + \nabla \cdot F(U) = 0$, which satisfy the gasdynamic scaling laws. This defines shock and contact surface trajectories: $r_s(t)$ and $r_0(t)$, respectively. Then in the “corrector step”, we integrate the linearized diffusion equations $\partial_t U = \mathcal{D} \nabla^2 U$ along the world lines¹: $r_0(t)$ or $r_s(t)$. Results are summarized in Table 1. Details will be provided in the manuscript.

4 Conclusions

Converged blast wave solutions are presented for 3 models: the inviscid, viscous and two-phase models. Away from the contact surface, the blast wave solutions for $\{p, \rho, T, u_r\}$ scale gasdynamically (i.e., with χ and τ of Table 1)— in agreement with the dimensional analysis of Bridgman (1922) and the similitude theory of Sedov (1943). However, molecular diffusion effects spread the contact surface and reduce the peak temperature in the shock-heated from $\sim 10,000 \text{ K}$ (inviscid) to $\sim 4,000 \text{ K}$ (viscous), as shown in Fig. 5. Such effects scale with the appropriately defined Peclet and Reynolds numbers of Table 1. The DP-air interface is unstable, and eventually evolves into a turbulent mixing layer (Fig. 6). This 3-D turbulent combustion simulation will also be presented.

Auspices

This work was performed under the auspices of the U.S. Department of Energy by Lawrence Livermore National Laboratory under Contract DE-AC52-07NA27344. Lawrence Livermore National Security. **LLNL-CONF-717199**.

¹ The Navier-Stokes terms have negligible effects in smooth regions of the flow, but major effects at discontinuities (see Fig. 3). Hence for scaling, it is sufficient to study diffusion effects along world lines.

Table 1. Scaling of Diffusion and Drag Effects

Effects	Model	Solution	Scaling Variable
<i>Inviscid</i>	$\partial_t U + \nabla \cdot F(U) = 0$	$U(\chi, \tau)$	$\chi \equiv \frac{r}{cm/g^{1/3}} \quad \& \quad \tau \equiv \frac{t \cdot a_0}{cm/g^{1/3}}$
<i>Mass Diffusivity</i> (at CS)	$Y_t = D_m Y_{rr}$	$Y_D(r, t) \rightarrow [1 + \text{erfc}\{\sqrt{Pe_m}/2\}]/2$	$Pe_m(r, t) \equiv \frac{\{r - r_0(t)\}^2}{D_m t}$
<i>Thermal Diffusivity</i> (at CS)	$T_t = D_Q T_{rr}$	$T(r, t) \rightarrow \frac{T_0}{\sqrt{4\pi D_Q t}} \exp\{-Pe_Q/4\pi\}$	$Pe_Q(r, t) \equiv \frac{\{r - r_0(t)\}^2}{D_Q t}$
<i>Viscosity</i> (at shock)	$u_t + uu_r = \nu u_{rr}$	$u(r, t) \rightarrow \frac{u_s}{1 + \exp\{Re/2\}}$	$Re(r, t) \equiv \frac{u_s \cdot \{r - r_s(t)\}}{\nu}$
<i>Drag</i>	$\dot{\mathbf{v}} = -K \mathbf{v}^2$	$\mathbf{v}(\tau) = -K \frac{v^0}{1 - \tau}$	$\tau \equiv (t - t_0) v^0$

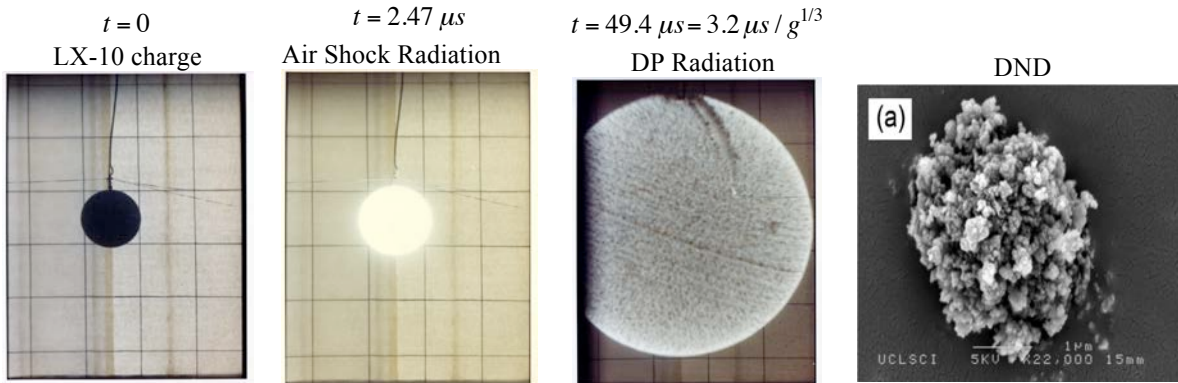


Figure 1. Photography of the early-time fireball from an 8-lb spherical LX-10 charge (Sauer, 1981); photograph of Detonation Nano Diamond (DND) agglomerate from a Comp B charge (Bevilacqua, 2008).

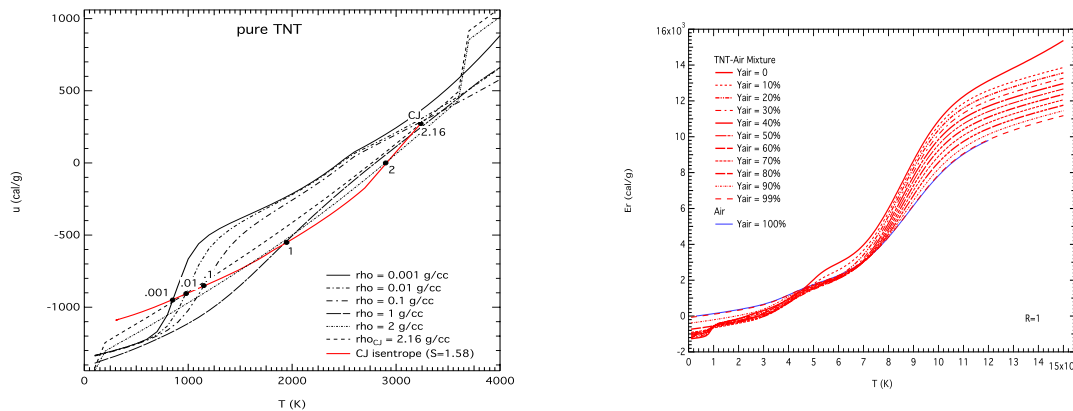


Figure 2. Equation of State in the internal energy—temperature plane for pure TNT and TNT-air mixtures, based on the thermodynamic equilibrium solution from the Cheetah code.

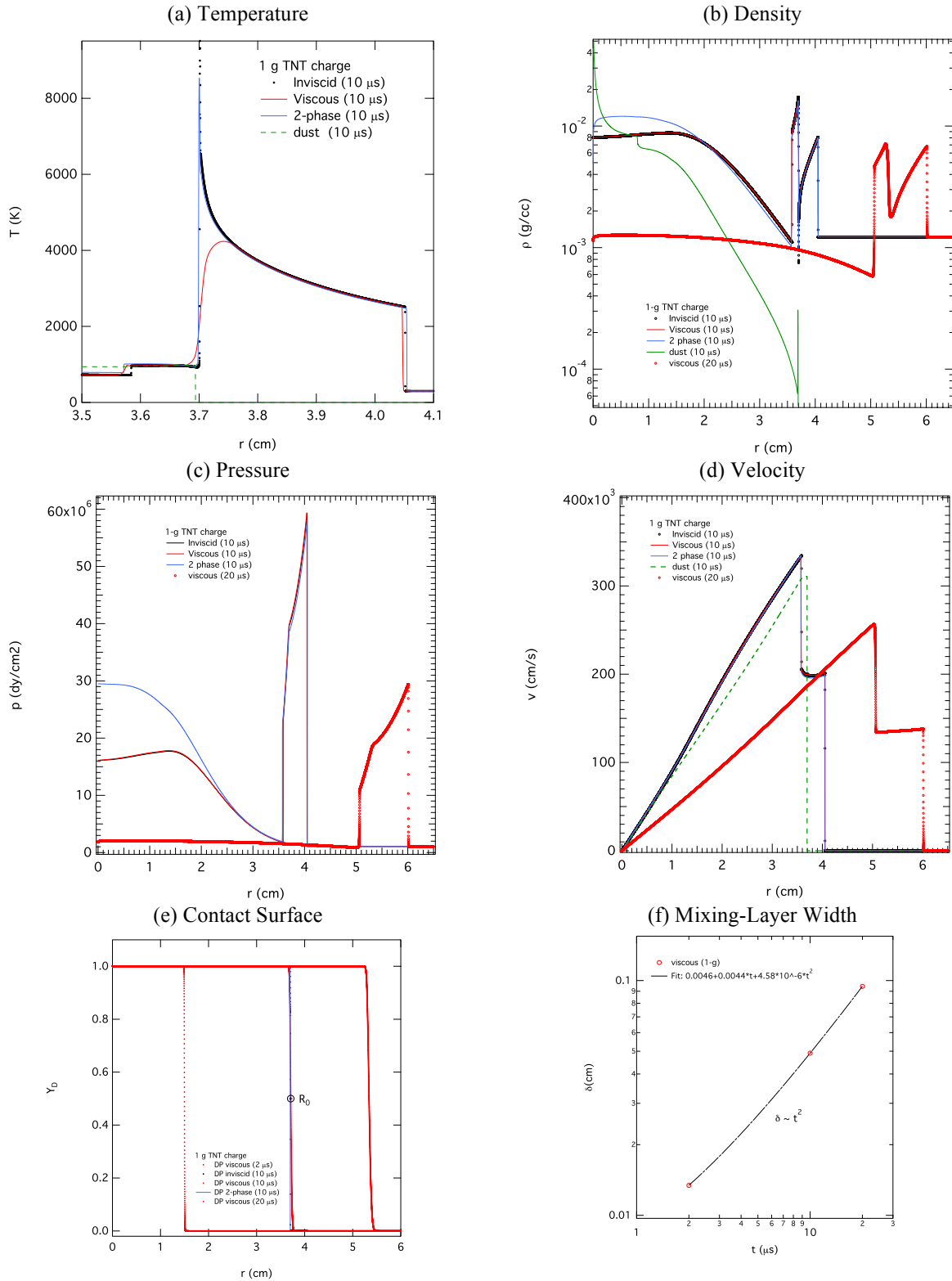


Figure 3. Evolution of the blast wave according to the inviscid, viscous and 2-phase models.

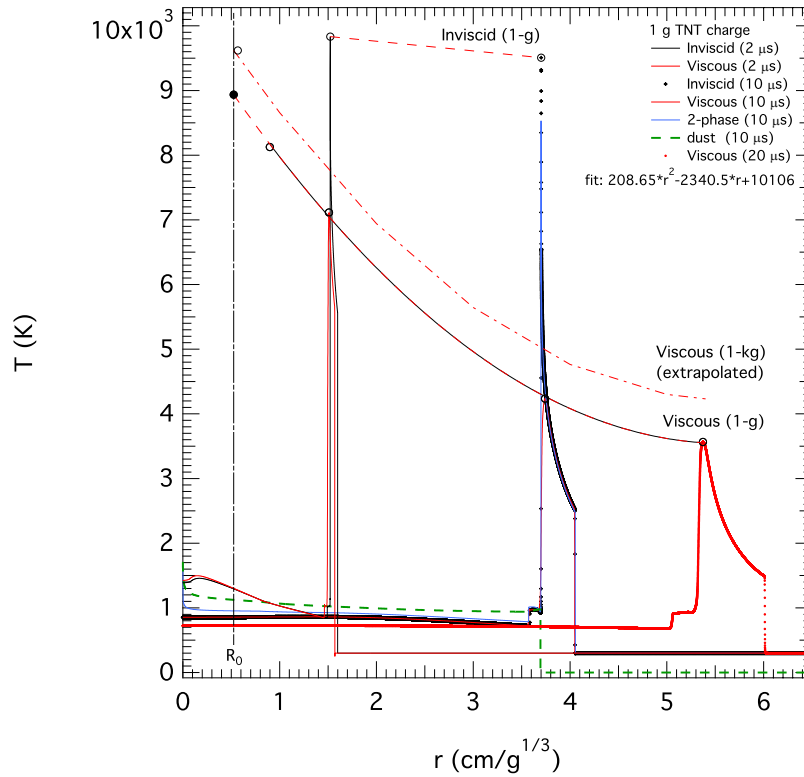


Figure 4. Comparison of inviscid and viscous solutions for a 1-g TNT charge, and extrapolation to a 1-kg charge.

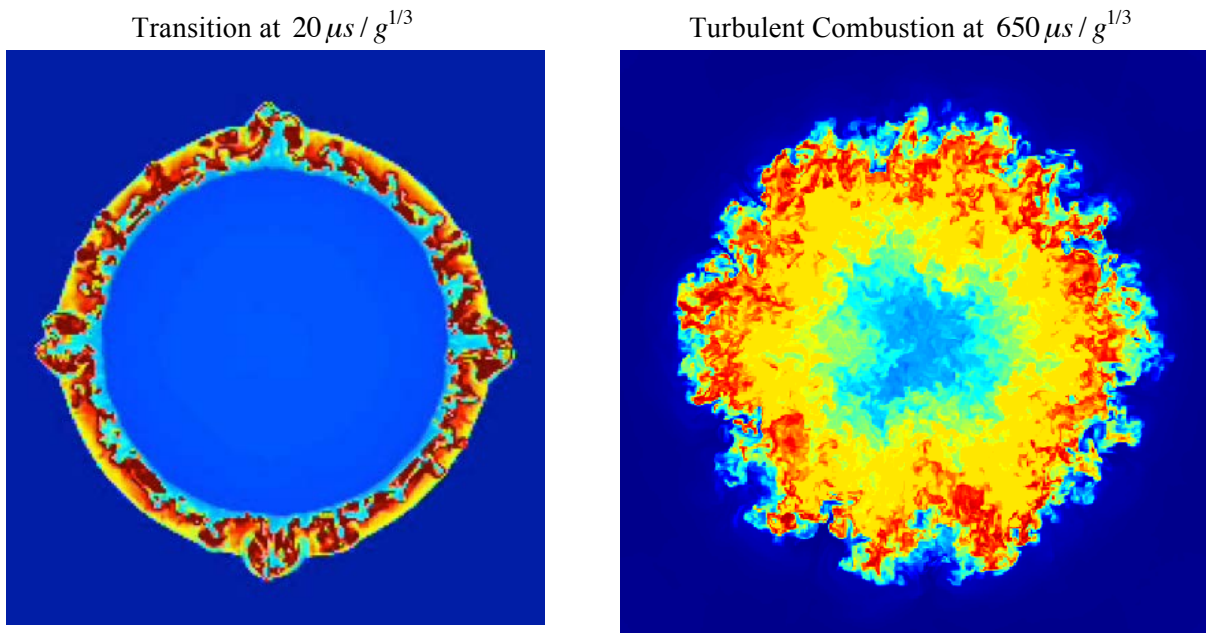


Figure 5. Temperature cross-section illustrating transition and turbulent combustion from an AMR code simulation of a 1-g TNT explosion in air.